

Generation of Quantum Entanglement in Autonomous Thermal Machines: Effects of Non-Markovianity, Hilbert Space Structure, and Quantum Coherence

A. Khoudiri,^{1,*} K. El Anouz,^{1,†} and A. El Allati^{1,‡}

¹*Laboratory of R&D in Engineering Sciences, Faculty of Sciences and Techniques Al-Hoceima, Abdelmalek Essaadi University, Tetouan, Morocco.*

We present a theoretical investigation of entanglement generation in an external quantum system interacting with a quantum autonomous thermal machine (QATM) under a non-Markovian dynamics. Indeed, the QATM is composed of two non-coupled qubits. Each qubit is coupled to an independent thermal reservoir, where each reservoir interacts with an external system of two additional non-coupled qubits. By analyzing the Hilbert space structure, energy level configurations, and temperature gradients, we define two thermodynamic cycles, namely A and B, governed by virtual temperatures and energy-conserving transitions. We demonstrate that the QATM can act as a structured reservoir able to induce non-Markovian memory effects. In fact, the non-Markovian dynamics is highlighted basically for negative entropy production rates. However, by quantitatively measuring the mutual information and concurrence, we show that the entanglement is generated only in cycle A, supported by the non-Markovian dynamics and strong presence of entanglement. Hence, we conclude that our results using feasible experimental parameters demonstrate that temperature differences, Hilbert space structure and coherence can be used as good quantum resources for controlling and boosting entanglement in quantum thermodynamic settings.

PACS numbers: 05.70.Ln, 05.30.-d 03.67.-a 42.50.Dv

I. INTRODUCTION

In the context of quantum thermodynamics, quantum autonomous thermal machines tie together quantum thermodynamic theory to quantum thermodynamic technologies [1–3]. The role of QATMs has been discussed in different frameworks, such as boosting quantum batteries and measuring low temperatures as quantum thermometry [4, 5]. Moreover, many-body systems correlations using QATMs are also investigated in [6]. In another context, many other works discussed quantum entanglement generation via QATMs, including maximal steady-state entanglement generation [7–9]. However, the entanglement generation using linear quantum thermal machines at low temperatures gives rise to a production of entanglement between environments [10]. Additionally, the Hilbert space structure that can be used as a quantum resource in the performance of multilevel quantum thermal machines is investigated in [11]. The QATMs also introduce the notion of virtual qubits and virtual temperature needed to investigate temperature reservoirs as quantum resources to ensure the autonomy of the machine [12, 13].

Importantly, in our recent work [15] the dynamical effect of a QATM on an external system, and the capability of the QATM to produce the memory effect based on the exchange of correlations with the external system were studied. Moreover, we presented the relationship between non-Markovianity and a generalized Landauer

bound principle [16] in the context of the autonomous quantum thermal machine. Through this relationship between quantum thermodynamics and quantum information theory using QATMs, we aim in this paper to study the entanglement generation using autonomous quantum thermal machines. Interestingly enough, the present paper is an expansion of our work in [15], linking the quantum thermodynamics framework with Hilbert space structure [16–18], non-Markovianity [19–22], virtual temperatures, and entanglement generation [23–26].

In our scenario, we study the dynamics of a quantum autonomous thermal machine composed of two qubits [12, 15]. This pair of qubits is defined as a non-coupled two-qubits interacting with two bosonic reservoirs, namely hot and cold ones. Moreover, we attach the QATM to a structured external system consisting of a non-coupled two-qubit system. Hence, we aim to investigate the Hilbert space structure of the QATM and external system qubits to realize the interaction between them based on temperature and energy constraints [11]. However, based on the concept of virtual temperature and virtual qubits of the QATM qubits [13], as well as the common interaction between the QATM and external system qubits, we realize two thermodynamical cycles, noted by A and B , allowing the examination of the difference between the reservoirs' temperatures and the Hilbert space structure. Mathematically, we provide the temperature transition between the cycles A and B with respect to the energy spacing of the QATM qubits. Numerically, we examine the validity of our theoretical framework with respect to the thermodynamical cycle, based on the heat and temperature dynamics of each subsystem [27]. In fact, to ensure the thermodynamic validity, we also examine

* khoudiri.achraf@etu.uae.ac.ma

† kelanouz@uae.ac.ma

‡ eabderrahim@uae.ac.ma

the second law of quantum thermodynamics through entropy production [28] to study the irreversibility of our system over time. Besides, we investigate the entropy production rate [29] to analyze the loss of information from the QATM and external system qubits into their reservoirs. Our results show that the entropy production rate is non-monotonic and attains negative values over time, indicating a non-Markovian behavior in our scenario. These results agree with those obtained by Popovic *et al.* [30], where negative entropy production rate is considered as a signature of non-Markovianity.

The above motivation allows us to explore the memory effect of cycles A and B [31]. We obtain that, even with the use of Markovian reservoirs, the non-Markovianity in our model appears due to the exchange of correlations between QATM and the external system over time, as shown also in [15, 30]. In addition, to show the effect of cycles A and B on entanglement generation, we measure the total (classical and quantum) correlation between the external system qubits using mutual information [32], and concurrence [33]. We find that total correlation is similar in both cycles, but the entanglement is generated only when the QATM operates in cycle A . This is according to the comparison between cycles A and B in terms of irreversibility and non-Markovianity over time. Hence, we conclude our analysis by discussing the effect of correlation coherence [34] and local coherences [35] on entanglement generation, showing that coherence represents a good quantum resource for producing quantum correlations over time in both cycles. Finally, it is worth mentioning that all our theoretical results are obtained using feasible experimental parameters [36–38].

Our paper is organized as follows: in Sec. II, we discuss our theoretical model; including the Hamiltonian description of the QATM and external system, QATM cycles, temperature and energy constraints. In Sec. III, we provide the dynamics of quantum thermodynamics, where Subsec. III A covers heat dynamics, QATM qubits and external system qubits. While temperatures, entropy production, and entropy production rate are treated in Subsec. III B and Subsec. III C, respectively. The memory effect of quantum thermal machine cycles and entanglement generation are discussed in Sec. IV. Finally, the non-Markovianity results are introduced in Subsec. IV A. Additionally, the generation of entanglement and the impact of correlation coherence are discussed in Subsec. IV B and Subsec. IV C, respectively, followed by the conclusion in Sec. V.

II. THEORETICAL FRAMEWORK: OPERATION CYCLE OF THE THERMAL MACHINE, TEMPERATURE AND ENERGY CONSTRAINTS

The proposed theoretical model consists of a QATM denoted by $M = M_1 \otimes M_2$, presented as a non-coupled two-qubit, M_1 and M_2 . Each qubit of the thermal machine is coupled to a Markovian bosonic reservoir called R_1 and R_2 , at temperatures T_{R_1} and T_{R_2} respectively. Moreover, the QATM M is coupled to an external system, namely $S = S_1 \otimes S_2$, which gives rise to a pair of non-coupled qubits denoted by S_1 and S_2 , respectively.

The idea behind proposing this model is related to the fact that we aim to investigate the role of the Hilbert space structure of the QATM, namely M and the external system S , as well as the difference between the temperatures T_{R_1} and T_{R_2} , to realize a thermodynamic cycles on the QATM. In this way, we can analyze how to enhance the memory effects in the external system S and how to improve the generation and control of entanglement.

A. Hamiltonian Framework and System Dynamics

The total Hamiltonian of our theoretical model is given in the following compact form,

$$\hat{H} = \hat{H}_M + \hat{H}_S + \hat{H}_R + \hat{H}_{MR} + \hat{H}_{MS}, \quad (1)$$

where \hat{H}_m ($m = \{M, S, R\}$) define the free Hamiltonian of the QATM, the external system S , and the reservoir $R = R_1 \otimes R_2$, respectively. Indeed, they are given as:

$$\begin{aligned} \hat{H}_M &= \sum_{i=1}^2 \hat{H}_{M_i}, & \hat{H}_{M_i} &= E_{M_i} \hat{\sigma}_{M_i}^\dagger \hat{\sigma}_{M_i}, \\ \hat{H}_S &= \sum_{i=1}^2 \hat{H}_{S_i}, & \hat{H}_{S_i} &= E_{S_i} \hat{\sigma}_{S_i}^\dagger \hat{\sigma}_{S_i}, \\ \hat{H}_R &= \sum_{i=1}^2 \hat{H}_{R_i}, & \hat{H}_{R_i} &= \sum_k E_{R_{ik}} \hat{a}_{R_{ik}}^\dagger \hat{a}_{R_{ik}}, \end{aligned}$$

where E_{M_i} and E_{S_i} for $i = \{1, 2\}$ are the spacing energy of the QATM qubits $M_1(M_2)$ and the external system subits $S_1(S_2)$ respectively. Moreover, $E_{R_{ik}}$ denotes the spacing energy of the reservoir R_i ($i = \{1, 2\}$) for each mode k of the set of bosonic harmonic oscillators. However, the raising and lowering operators of the QATM and the external system are defined as $\hat{\sigma}_{M_i(S_i)} = |0\rangle_{M_i(S_i)} \langle 1|$ and $\hat{\sigma}_{M_i(S_i)}^\dagger = |1\rangle_{M_i(S_i)} \langle 0|$, which satisfying: $\hat{\sigma}_{M_i(S_i)} |1\rangle_{M_i(S_i)} = |0\rangle_{M_i(S_i)}$ and $\hat{\sigma}_{M_i(S_i)}^\dagger |0\rangle_{M_i(S_i)} = |1\rangle_{M_i(S_i)}$, respectively. However, $\hat{a}_{R_{ik}}$ ($\hat{a}_{R_{ik}}^\dagger$) are the annihilation and creation operators of the reservoir R_i for the harmonic oscillator mode k .

Now, the interaction between each reservoir R_1 (R_2) and the QATM qubits M_1 (M_2) is described under the rotating wave approximation ($E_{M_i} = E_{R_{ik}}$) using the following interaction Hamiltonian:

$$\hat{H}_{MR} = \sum_{i=1}^2 \sum_k g_{ik} (\hat{\sigma}_{M_i} \hat{a}_{ik}^\dagger + H.c.). \quad (2)$$

Here, g_{ik} is the coupling rate between the reservoir R_i and the qubit M_i for $i = \{1, 2\}$. The Hamiltonian \hat{H}_{MS} represents the interaction between the QATM $M = M_1 \otimes M_2$ and the external system $S = S_1 \otimes S_2$ that we will report later. According to this interaction, we will define the quantum thermodynamical cycles of the QATM in the next subsection. For this model, we propose the initial state, namely $\hat{\rho}(0)$, as follows:

$$\hat{\rho}(0) = \hat{\rho}_{R_1-M_1}(0) \otimes \hat{\rho}_{R_2-M_2}(0) \otimes \hat{\rho}_S(0). \quad (3)$$

Note that initially no correlation between each subsystem is considered, meaning that $\hat{\rho}_{R_i-M_i}(0) = \hat{\rho}_{R_i}(0) \otimes \hat{\rho}_{M_i}(0)$ for $i = \{1, 2\}$, where $\hat{\rho}_{R_i}(0)$ and $\hat{\rho}_{M_i}(0)$ are the initial states of the subsystems R_i and M_i , respectively. However, the initial state of the external system is given as $\hat{\rho}_S(0) = \hat{\rho}_{S_1}(0) \otimes \hat{\rho}_{S_2}(0)$. In this regards, under the weak interaction between the QATM $M = M_1 \otimes M_2$ and the reservoirs R_1 and R_2 , the total system evolves as $\hat{\rho}(t) = \hat{U}(t) \hat{\rho}(0) \hat{U}^\dagger(t)$, where $\hat{U}(t) = \exp(-j\hat{H}t)$ (with $\hbar = 1$). Hence, one can use the local standard Born-Markov master equation in its Lindblad form:

$$\frac{d}{dt} \hat{\rho}(t) = -j [\hat{H}_S + \hat{H}_M, \hat{\rho}(t)] + \mathcal{L}[\hat{\rho}(t)], \quad (4)$$

where the first term on the right-hand of Eq.(4) describes the free evolution of the subsystems M and the external system S , which is the reversible part of the evolution of our theoretical model. However, $\mathcal{L}[\hat{\rho}(t)]$ denotes the dissipative (irreversible) part, describing the decoherence effects of the reservoirs R_1 and R_2 into M and S . Indeed, it is defined as:

$$\begin{aligned} \mathcal{L}[\hat{\rho}(t)] &= -j [\hat{H}_{MS}, \hat{\rho}(t)] + \sum_{i=1}^2 \mathcal{D}^{[T_{M_i}]}[\hat{\rho}(t)], \\ \mathcal{D}^{[T_{M_i}]}[\hat{\rho}(t)] &= \gamma_i (\bar{n}_i(T_{M_i}, E_{M_i}) + 1) \mathcal{D}^{[\hat{\sigma}_{M_i}]}[\hat{\rho}(t)] \\ &\quad + \gamma_i \bar{n}_i(T_{M_i}, E_{M_i}) \mathcal{D}^{[\hat{\sigma}_{M_i}^\dagger]}[\hat{\rho}(t)], \\ \mathcal{D}^{[\hat{\sigma}_{M_i}^\dagger]}[\hat{\rho}(t)] &= \hat{\sigma}_{M_i}^\dagger \hat{\rho}(t) \hat{\sigma}_{M_i} - \frac{1}{2} \{ \hat{\sigma}_{M_i} \hat{\sigma}_{M_i}^\dagger, \hat{\rho}(t) \}, \\ \mathcal{D}^{[\hat{\sigma}_{M_i}]}[\hat{\rho}(t)] &= \hat{\sigma}_{M_i} \hat{\rho}(t) \hat{\sigma}_{M_i}^\dagger - \frac{1}{2} \{ \hat{\sigma}_{M_i}^\dagger \hat{\sigma}_{M_i}, \hat{\rho}(t) \}, \end{aligned} \quad (5)$$

where γ_i denotes the dissipation rate, $\bar{n}_i(T_{M_i}, E_{M_i})$ is the average number of the set of harmonic oscillators in the thermal bosonic reservoir R_i at the temperature T_{M_i} of the corresponding gap of energy E_{M_i} which is defined as:

$$\bar{n}(T_{M_i}, E_{M_i}) = \frac{1}{\exp(\frac{E_{M_i}}{T_{M_i}}) - 1}, \quad \text{for } i = \{1, 2\}. \quad (6)$$

In the next subsection, we shall describe the interaction between the QATM $M = M_1 \otimes M_2$ and the external system $S = S_1 \otimes S_2$, where we can investigate the Hilbert space structure of each subsystem M and S , the difference between the temperatures T_{M_1} and T_{M_2} as a quantum thermodynamic resources for realizing a thermodynamic cycle of the quantum autonomous thermal machine M .

B. Quantum Thermal Machine Cycles

The objective of this subsection is to define the QATM M , and to investigate the difference in temperature reservoirs R_1 (R_2) and the Hilbert space structure of each subsystem M and S as a resource to operate the QATM M autonomously without any external injection of work. The QATM qubits M_1 and M_2 are in thermal equilibrium with their respective reservoirs R_1 and R_2 at temperatures $T_{R_i} = T_{M_i}$ for $i = \{1, 2\}$. They are defined by the Boltzmann distribution in their thermal states (we set the Boltzmann constant $K_B = 1$) as:

$$\begin{aligned} \hat{\rho}_{M_i}(0) &= \frac{1}{Z_{M_i}} e^{-\frac{\hat{H}_{M_i}}{T_{M_i}}}, \quad i = \{1, 2\}, \\ \hat{\rho}_M(0) &= \hat{\rho}_{M_1}(0) \otimes \hat{\rho}_{M_2}(0), \end{aligned} \quad (7)$$

where $Z_{M_i} = \text{Tr}_{M_i} \{ e^{-\frac{\hat{H}_{M_i}}{T_{M_i}}} \}$ is the partition function of the thermal machine qubit M_i for $i = \{1, 2\}$, and $\hat{\rho}_M(0)$ is the initial state of the QATM. Note that the reservoirs R_1 and R_2 are the cold and hot reservoirs, respectively, with $T_{M_1} \leq T_{M_2}$. We set the energy spacing of each qubit M_1 and M_2 satisfying $E_{M_2} > E_{M_1}$.

The coupling between the reservoir R_i and the QATM qubit M_i , for $i = \{1, 2\}$, biases the transition from $|0\rangle_{M_i}$ to $|1\rangle_{M_i}$, consisting of an increase in the excited-state probability of M_i , or from $|1\rangle_{M_i}$ to $|0\rangle_{M_i}$, consisting of a decrease in the excited-state probability of M_i , meaning the heating or cooling of the qubit M_i , respectively. Now, let define the heat Q_{M_i} and Q_{S_i} of the QATM qubit M_i and the external system qubit S_i as:

$$\begin{aligned} Q_{M_i} &= \text{Tr}_{M_i} \{ \hat{H}_{M_i} (\hat{\rho}_{M_i}(t) - \hat{\rho}_{M_i}(0)) \}, \\ Q_{S_i} &= \text{Tr}_{S_i} \{ \hat{H}_{S_i} (\hat{\rho}_{S_i}(t) - \hat{\rho}_{S_i}(0)) \}, \quad i = \{1, 2\}. \end{aligned} \quad (8)$$

Now, let's investigate the interaction between the reservoirs R_1 (R_2), the QATM $M = M_1 \otimes M_2$, and the external system $S = S_1 \otimes S_2$, the impact of temperature and Hilbert space structure of S and M to realize two thermodynamical cycles on the QATM. Indeed, these cycles are called as cycle *A* cycle *B*, which are defined as follows:

- **Cycle A:** consists of the transition from $|0_{M_1} 0_{M_2}\rangle$ and $|0_{M_1} 1_{M_2}\rangle$ to $|1_{M_1} 0_{M_2}\rangle$ and $|1_{M_1} 1_{M_2}\rangle$, under the heating of the qubit M_1 according to the coupling with R_1 , which corresponds to $Q_{M_1}(t) \geq 0$. Moreover, the transition from $|0_{M_1} 1_{M_2}\rangle$ and $|1_{M_1} 1_{M_2}\rangle$

to $|0_{M_1}0_{M_2}\rangle$ and $|1_{M_1}0_{M_2}\rangle$, which corresponds to the cooling of the qubit M_2 under the interaction with R_2 , $Q_{M_2} \leq 0$. To close the thermodynamical cycle, the QATM $M = M_1 \otimes M_2$ loses heat into the external system $S = S_1 \otimes S_2$, which corresponds to the transition from $|1_{M_1}0_{M_2}\rangle \otimes |0_{S_1}1_{S_2}\rangle$ to $|0_{M_1}1_{S_2}\rangle \otimes |1_{M_1}0_{S_2}\rangle$ as shown in Fig. (1b). This cycle imposes the following condition of conservation of energy :

$$\begin{aligned} E(|1_{M_1}0_{M_2}0_{S_1}1_{S_2}\rangle) &= E(|0_{M_1}1_{S_2}1_{M_1}0_{S_2}\rangle), \\ E_{M_2} - E_{M_1} &= E_{S_2} - E_{S_1}. \end{aligned} \quad (9)$$

Note that the above condition in Eq. (9) is a necessary condition used to verify cycle *A* over time.

- **Cycle B:** consists of the transition from $|0_{M_1}0_{M_2}\rangle$ and $|1_{M_1}0_{M_2}\rangle$ to $|0_{M_1}1_{M_2}\rangle$ and $|1_{M_1}1_{M_2}\rangle$, under the heating of the qubit M_2 according to the coupling with R_2 , which corresponds to $Q_{M_2}(t) \geq 0$. Moreover, transition from $|1_{M_1}0_{M_2}\rangle$ and $|1_{M_1}1_{M_2}\rangle$ to $|0_{M_1}0_{M_2}\rangle$ and $|0_{M_1}1_{M_2}\rangle$, which corresponds to the cooling of the qubit M_1 under the interaction with R_1 , $Q_{M_1} \leq 0$. Again to close the thermodynamical cycle, the QATM $M = M_1 \otimes M_2$ loses heat into the external system $S = S_1 \otimes S_2$, which corresponds to the transition from $|0_{M_1}1_{M_2}\rangle \otimes |1_{S_1}0_{S_2}\rangle$ to $|1_{M_1}0_{M_2}\rangle \otimes |0_{S_1}1_{S_2}\rangle$ as shown in Fig. (1a). This cycle imposes the condition of conservation of energy, such that:

$$\begin{aligned} E(|0_{M_1}1_{M_2}1_{S_1}0_{S_2}\rangle) &= E(|1_{M_1}0_{M_2}0_{S_1}1_{S_2}\rangle), \\ E_{M_2} - E_{M_1} &= E_{S_2} - E_{S_1}. \end{aligned} \quad (10)$$

The above condition in Eq. (10) is a necessary condition to verify Cycle *B* over time.

The QATM $M = M_1 \otimes M_2$ and the external system $S = S_1 \otimes S_2$, under the conditions in Eqs. (9) and (10) bias the transitions $|0_{M_1}1_{M_2}\rangle \otimes |1_{S_1}0_{S_2}\rangle \leftrightarrow |1_{M_1}0_{M_2}\rangle \otimes |0_{S_1}1_{S_2}\rangle$, meaning that the interaction Hamiltonian \hat{H}_{MS} is defined as:

$$\hat{H}_{MS} = g(|0_{M_1}1_{M_2}1_{S_1}0_{S_2}\rangle \langle 1_{M_1}0_{M_2}0_{S_1}1_{S_2}| + H.c), \quad (11)$$

where g is the coupling coefficient between QATM, namely M and the external system S .

C. Temperature and Energy Constraints

As we have already mentioned before, the main subject of this work is to investigate the Hilbert space structure and the exchange of excitation as heat between the subsystems M_i and S_i and the reservoir R_i for $i = \{1, 2\}$, under the condition of energy conservation in Eqs. (9) and (10), to define the cycles A and B, respectively. Note

that the QATM $M = M_1 \otimes M_2$ and the external system $S = S_1 \otimes S_2$ are operated as a single body of energy spacing $E_M = E_S = E_{M_2} - E_{M_1}$, with the ground and excited states being $|0\rangle_{M(S)} = |1_{M_1(S_1)}0_{M_2(S_2)}\rangle$ and $|1\rangle_{M(S)} = |0_{M_1(S_1)}1_{M_2(S_2)}\rangle$, respectively. The populations of the excited and ground states, namely $P_{M(S)}^E(t)$ and $P_{M(S)}^G(t)$ are straightforwardly defined as:

$$P_{M(S)}^G(t) = P_{M_1(S_1)}^E(t)P_{M_2(S_2)}^G(t), \quad (12)$$

$$P_{M(S)}^E(t) = P_{M_1(S_1)}^G(t)P_{M_2(S_2)}^E(t), \quad (13)$$

where $P_{M_i(S_i)}^G(t) = \langle 0_{M_i(S_i)} | \hat{\rho}_{M_i(S_i)}(t) | 0_{M_i(S_i)} \rangle$ and $P_{M_i(S_i)}^E(t) = \langle 1_{M_i(S_i)} | \hat{\rho}_{M_i(S_i)}(t) | 1_{M_i(S_i)} \rangle$ are the ground and excited state populations of the qubit $M_i(S_i)$ for $i = \{1, 2\}$, respectively. In the context of quantum thermodynamics, the QATM M and the external system S are treated as a single body, namely a virtual qubit. Since the QATM qubits M_1 and M_2 follow Boltzmann distributions, one can write:

$$\begin{aligned} P_{M_i}^E(t) &= P_{M_i}^G(t) e^{-\frac{E_{M_i}}{T_{M_i}}}, \quad (i = \{1, 2\}), \\ P_M^E(t) &= P_M^G(t) e^{-\frac{E_M}{T_M}}. \end{aligned} \quad (14)$$

Here, E_M denotes the energy level spacing of the QATM when it is treated as a single body, at the virtual temperature denoted T_M . It is defined as:

$$T_M = \frac{E_M}{\frac{E_{M_2}}{T_{M_2}} - \frac{E_{M_1}}{T_{M_1}}}. \quad (15)$$

It is worth mentioning that the virtual temperature of the QATM, namely T_M is not the average of the temperatures T_{M_1} and T_{M_2} . At equilibrium, we have $T_M = T_{M_1} = T_{M_2}$, and it is an important parameter used to define the constraint on temperature that differentiates between cycle *A* and cycle *B*. Moreover, the latter ones are closed under the exchange of heat between the QATM M and the external S , corresponding to the transition $|0\rangle_M \leftrightarrow |1\rangle_M$, with the exchanged heat of the QATM M where it acts as a single body is noted $Q_M(t)$ which is defined as:

$$Q_M(t) = E_M(P_M^E(t) - P_M^E(0)). \quad (16)$$

Hence, the virtual temperature for both cycles *A* and *B* are detailed as bellow:

- **Cycle A:** consists of heat gain from the external system S into the QATM, meaning that $Q_M(t) \geq 0$, which implies that an increase in the excited state probability of the QATM, M ($P_M^E(t) \geq P_M^E(0)$). In addition, using Eqs. (14) and (15), we find that the virtual temperature of the QATM M in cycle *A* evolves negatively over time, namely $T_M \leq 0$. Therefore, we obtain the constraint on the temperatures T_{M_1} and T_{M_2} for realizing cycle A as:

$$T_{M_1} \leq \frac{E_{M_1}}{E_{M_2}} T_{M_2}. \quad (17)$$

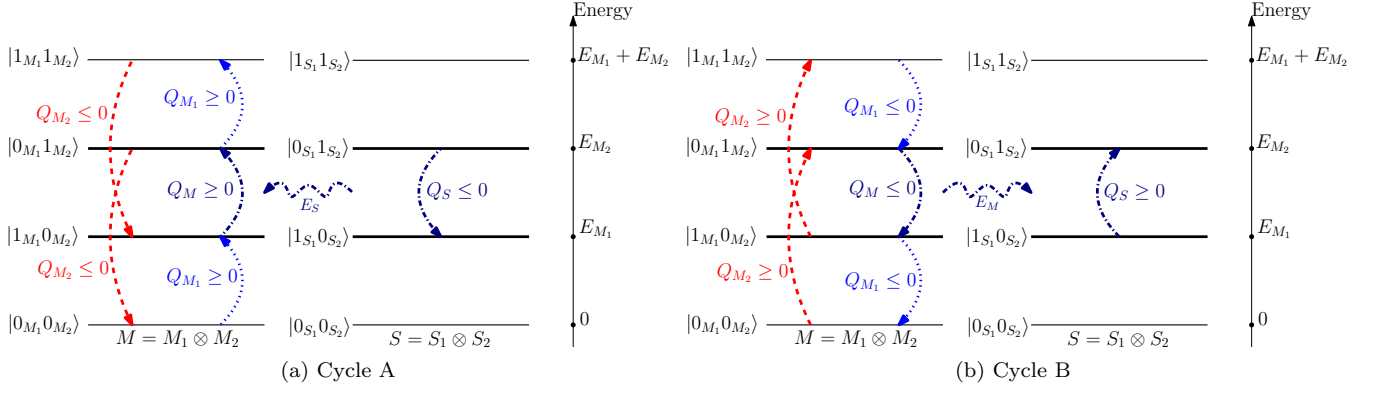


FIG. 1. (a) Schematic representation of the cycle A of the QATM: heating of qubit M_1 and cooling of qubit M_2 with heat transfer from the external system to the machine. (b) Cycle B: heating of qubit M_2 and cooling of qubit M_1 with heat transfer from the machine to the external system. The arrows indicate the direction of heat flow between QATM qubits, thermal reservoirs, and the external system.

- **Cycle B:** consists of heat gain using the external system S from the QATM M , meaning that $Q_M(t) \leq 0$, which implies a decrease in the excited state probability of the QATM ($P_M^E(t) \leq P_M^E(0)$). In fact, using Eqs. (14) and (15), we obtain that the virtual temperature of the QATM M in cycle B, which evolves positively over time, namely $T_M \geq 0$. Therefore, one can obtain the constraint on the temperatures T_{M_1} and T_{M_2} for realizing cycle B as:

$$T_{M_1} \geq \frac{E_{M_1}}{E_{M_2}} T_{M_2}. \quad (18)$$

Theoretically, we show that the constraints on the energies of the QATM qubits and the external system qubits satisfy the conditions in Eqs. (9) and (10). In the rest of the paper, for the sake of simplicity, we set $E_{M_i} = E_{S_i}$ for $i = \{1, 2\}$. The temperature constraints required to realize the transition between cycles A and B are given in Eqs. (17) and (18).

However, for the numerical results, we normalize the energy scale by setting $E_{M_2} = 10$ and we choose $E_{M_1} = 5$. Moreover, the transition point between cycles A and B in terms of temperature occurs at $T_{M_1} = 0.5T_{M_2}$, with dissipation rates $\gamma_i = 0.1$ for $i = \{1, 2\}$. Note that in the following, we use $T_{M_1} = 0.1T_{M_2}$ for cycle A and $T_{M_1} = 0.8T_{M_2}$ for cycle B, with $T_{M_2} = 1$. While the range of the coupling between the QATM M and the external system S is chosen as $g = 0.3, 0.5, 0.$, and 0.9 . Interestingly enough, note that these parameters are used to map between the theoretical framework and the experimental realization. For instance, in superconducting qubits [36–38], the energy spacing fluctuates typically between 4 GHz and 10 GHz. In natural units ($\hbar = 1$), using $E_{M_2} = 10$ is equivalent to operating in the GHz range. While the coupling g in experimental studies ranges between 10 MHz and 100 MHz. Finally, the relevant time

scale takes the values between 20 μs and 200 μs . Hence, these considerations prove that our model is experimentally realizable and represents a realistic system.

III. DYNAMICS OF QUANTUM THERMODYNAMIC QUANTITIES: HEAT AND TEMPERATURE

In this section, we numerically manipulate the constraints provided in Eqs. (17) and (18) on the dynamics of heat and temperatures of each subsystem. Indeed, we have used the initial state for the QATM, the density matrix given in Eq. (7). Moreover, for the external system S in the rest of the paper, we use the superposition state $|\psi(0)\rangle_{S_1} = \frac{1}{\sqrt{2}}(|0\rangle_{S_1} + |1\rangle_{S_1})$ for qubit S_1 and $|\psi(0)\rangle_{S_2} = \frac{1}{\sqrt{2}}(|0\rangle_{S_2} - |1\rangle_{S_2})$ for qubit S_2 . Hence, the corresponding initial density matrix is given as: $\hat{\rho}_{S_i}(0) = |\psi(0)\rangle_{S_i} \langle\psi(0)|$ for $i = \{1, 2\}$.

A. Heat dynamics

Here, we investigate the definition of heat in Eq. (8) to examine the dynamics of heat for the QATM qubits M_1 and M_2 , namely $Q_{M_1}(t)$ and $Q_{M_2}(t)$ respectively. Moreover, we evaluate the dynamics of heat for the external system qubits S_1 and S_2 , i.e., $Q_{S_1}(t)$ and $Q_{S_2}(t)$ respectively. However, we set the coupling between the QATM and the external system S as $g = 0.09$. While the temperature of the qubit M_2 is chosen as $T_{M_2} = 1$. Then the heat as a function of time and the temperature T_{M_1} in the interval $T_{M_1} \in [0.1T_{M_2}, T_{M_2}]$ is plotted in the following contour plots.

The variations of heat for the QATM qubits, namely $Q_{M_1}(t)$ and $Q_{M_2}(t)$ are shown in Figs. (2a) and (2b), respectively. We observe that in the case where $T_{M_1} \leq$

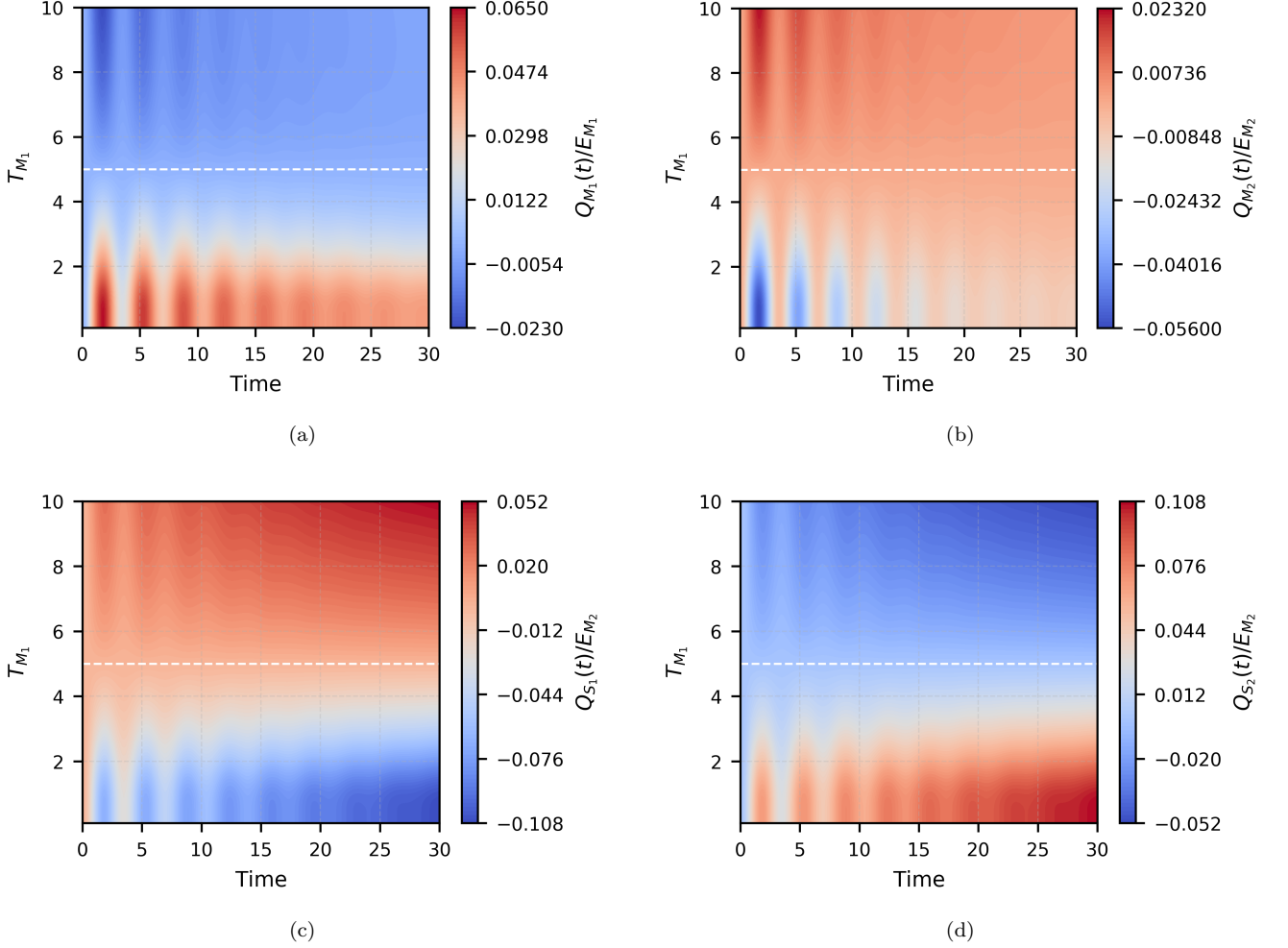


FIG. 2. (a,b): plot of heat for each qubit of QATM, namely M_1 and M_2 . Moreover, (c,d): plot of heat for each qubit of the external system, namely S_1 and S_2 . The two regions are separated by the white dashed line, which corresponds to the ratio T_{M_1}/T_{M_2} using Eqs.(17) and (18).

$0.5T_{M_2}$, the heat satisfies $Q_{M_1}(t) \geq 0$ and $Q_{M_2}(t) \leq 0$. While, in the case of $T_{M_1} \geq 0.5T_{M_2}$, the heat satisfies $Q_{M_1}(t) \leq 0$ and $Q_{M_2}(t) \geq 0$. Physically, this behavior corresponds to the conditions of transition between cycles A and B in Eqs. (17) and (18). However, for the external system qubits, namely S_1 and S_2 , the heat variations are given in Figs. (2c) and (2d), respectively. Obviously, in the case of $T_{M_1} \leq 0.5T_{M_2}$ (cycle A), the heats satisfy $Q_{S_1}(t) \leq 0$ and $Q_{S_2}(t) \geq 0$. But, in the case of $T_{M_1} \geq 0.5T_{M_2}$ (cycle B), the heats satisfy $Q_{S_1}(t) \geq 0$ and $Q_{S_2}(t) \leq 0$. Concerning the variation of the heat of the QATM qubits, namely $Q_{M_i}(t)$ for $i \in \{1, 2\}$, under the condition of resonance between the qubits M_i and S_i ($E_{M_i} = E_{S_i}$), one can observe that the heat is partially exchanged as $Q_{S_i}(t) \rightarrow Q_{M_i}(t)$ for cycle A. While, it is exchanged as $Q_{M_i}(t) \rightarrow Q_{S_i}(t)$ for cycle B. Finally, the non-monotonic behavior of the heat dynamics for $Q_{M_i}(t)$ and $Q_{S_i}(t)$ is due to the memory effects of the proposed model, as we will show in the next section.

B. Temperature dynamics

In this part, we aim to show the dynamics of the temperatures of each qubit of the QATM, namely T_{M_i} for the qubits M_i with $i \in \{1, 2\}$. Moreover, the dynamics of the total virtual temperature of the whole QATM, that is, T_M . Indeed, to achieve this goal, we use Eq. (14) to obtain the following formulas:

$$T_{M_i}(t) = \frac{E_{M_i}}{\ln(P_{M_i}^G(t)) - \ln(P_{M_i}^E(t))}, \quad (i \in \{1, 2\}),$$

$$T_M(t) = \frac{E_M}{\ln(P_M^G(t)) - \ln(P_M^E(t))}. \quad (19)$$

For cycle A, in Fig. (3a), the temperatures are initially given as: $T_{M_1} = 0.1T_{M_2}$, $T_{M_2} = 1$, and $T_M \leq 0$. Obviously, the temperature of the qubit M_1 increases, while that of M_2 decreases, as reflected in the obtained results of heat transfer shown in Figs. (2a) and (2b), under

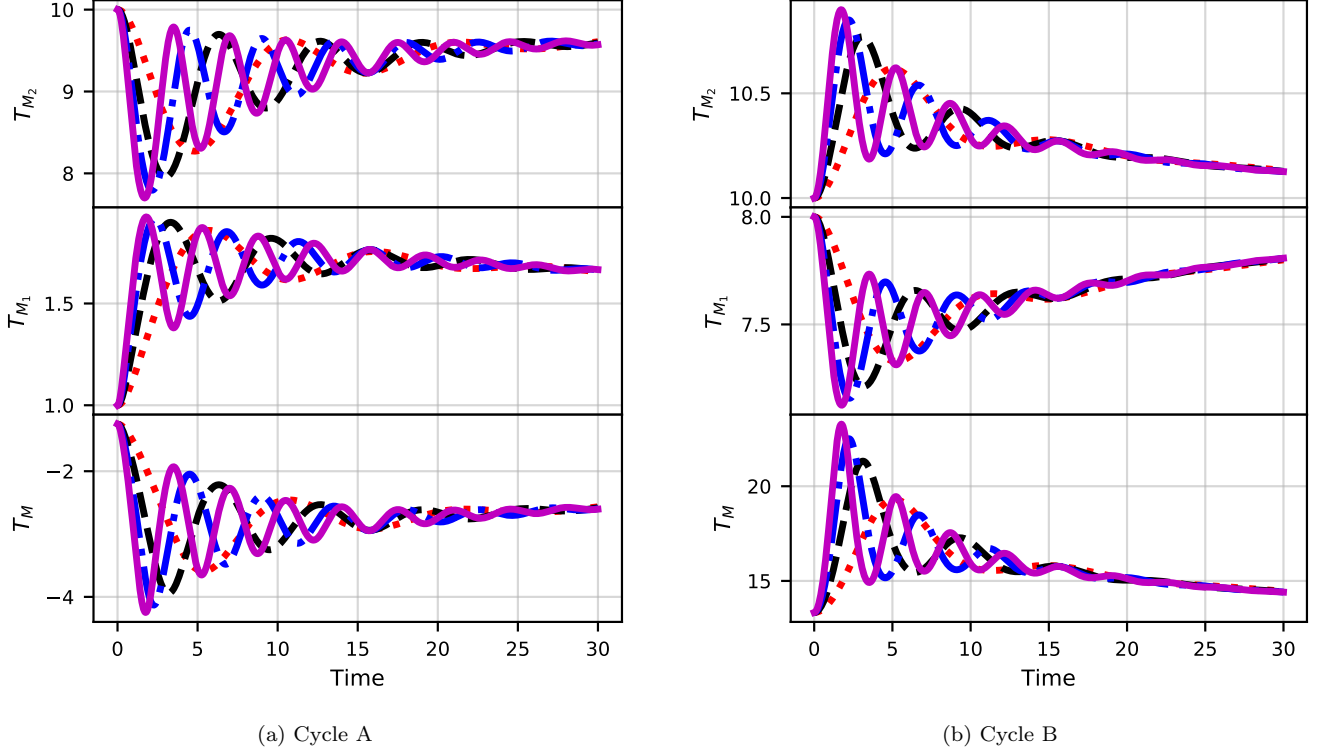


FIG. 3. Temperature evolution of each qubit of QATM and total temperature of the whole QATM over time. (a) Cycle A: a clear gradual increase of T_{M_1} and a decrease of T_{M_2} with a negative virtual temperature $T_M < 0$ is observed. (b) Cycle B: a decrease of T_{M_1} and an increase of T_{M_2} with a positive virtual temperature $T_M > 0$ is shown. The coupling strength is varied in units of E_{M_2} as $g = 0.03, 0.05, 0.07$, and 0.09 for red, black, blue and magenta curves.

the condition given in Eq. (17). Physically speaking, during the transition of qubit M_1 from $|0\rangle_{M_1}$ to $|1\rangle_{M_1}$, a positive heat $Q_{M_1}(t) \neq 0$ from its reservoir R_1 is gained. Whereas, for qubit M_2 , during the transition from $|1\rangle_{M_2}$ to $|0\rangle_{M_2}$ there is a loss of heat to its reservoir R_2 , namely $Q_{M_2}(t) \leq 0$. Then, the QATM M gains heat $Q_M \geq 0$ from the external system S at the virtual temperature T_v .

However, for cycle B, in Fig. (3b), the temperatures are initially given as: $T_{M_1} = 0.8T_{M_2}$, $T_{M_2} = 1$, and $T_M \geq 0$. It is clear that the temperature of qubit M_1 decreases under the exchange of positive heat $Q_{M_1}(t) \geq 0$ with its reservoir R_1 (cooling). However, the temperature of qubit M_2 increases under the exchange of negative heat $Q_{M_2}(t) \leq 0$ with its reservoir R_2 (heating), satisfying always the condition in Eq. (18). In addition, the non-monotonic evolution of the qubit temperatures via increasing the coupling between the QATM and external system S is due to the memory effect, which consists of information exchanged between them. Note that the obtained negative values of the virtual temperature are physical, as it is associated with population inversion (like in lasers). Indeed, the virtual temperature plays a fascinating, important role in complex quantum thermodynamic systems, allowing for the differentiation between types of thermal machines.

C. Entropy production and entropy production rate

The quantum entropy production and entropy production rate, namely $\Sigma(t)$ and $\sigma(t) = \dot{\Sigma}(t)$, respectively, are important concepts in quantum thermodynamics. Indeed, they quantify the irreversibility of the open system over time. Moreover, it can also be interpreted as the loss of information of the system to its environment. Mathematically, they take the following compact form:

$$\Sigma(t) = \Delta S(\hat{\rho}(t)) - \sum_{i=1}^2 \frac{\Delta Q_{M_i}(t)}{T_{M_i}(t)}, \quad (20)$$

$$\sigma(t) = \frac{d}{dt}\Sigma(t). \quad (21)$$

Here, $S(\hat{\rho}(t)) = -\text{Tr}\{\hat{\rho}(t) \log_2[\hat{\rho}(t)]\}$ denotes the von-Neumann entropy of the total density matrix of our theoretical model. Besides, we define $\Delta S(\hat{\rho}(t)) = S(\hat{\rho}(t)) - S(\hat{\rho}(0))$ and $\Delta Q_{M_i}(t) = Q_{M_i}(t) - Q_{M_i}(0) = Q_{M_i}(t)$ for the thermal machine qubit M_i , with $i = \{1, 2\}$.

In Fig. (4), we analyze the entropy production and entropy production rate versus time for various considerations of the coupling strength between the QATM and

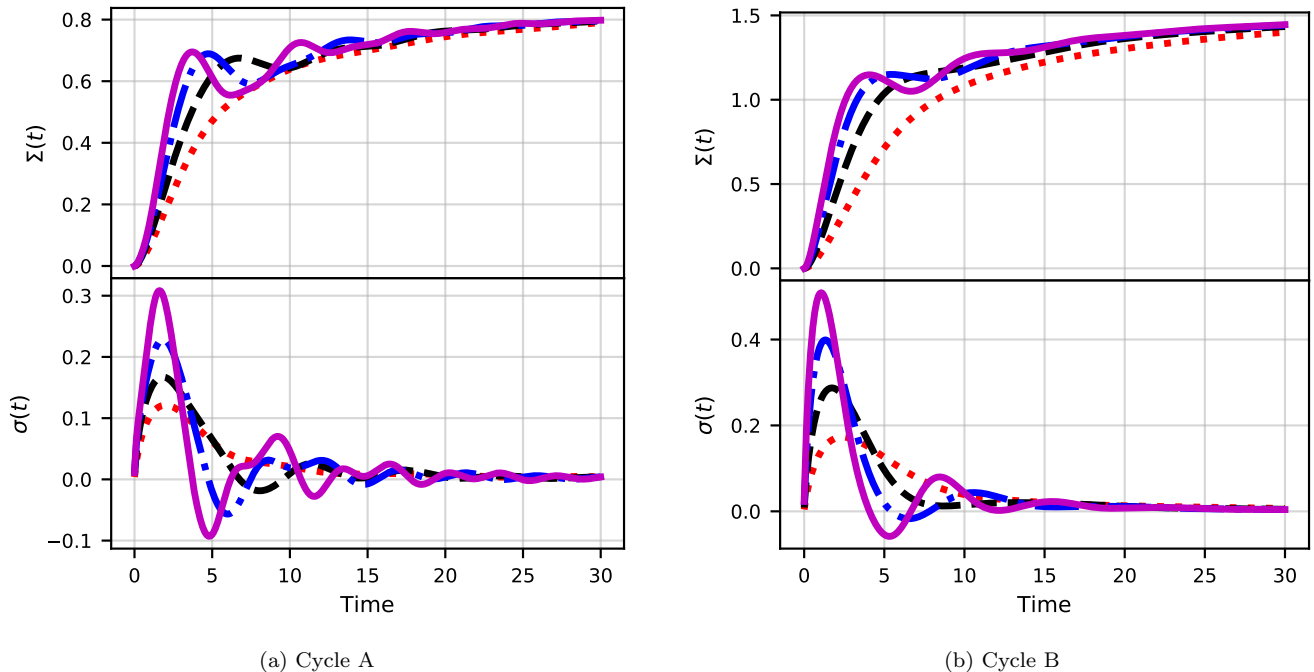


FIG. 4. Entropy production $\Sigma(t)$ and entropy production rate $\sigma(t)$ versus time. (a) Cycle A: smaller entropy production with more frequent and stronger negative rates, indicating robust non-Markovianity. (b) Cycle B: larger entropy production with less frequent negative rates, indicating small non-Markovianity. The coupling strength is varied in units of E_{M_2} as $g = 0.03, 0.05, 0.07$, and 0.09 for red, black, blue and magenta curves.

the external system S , for cycles A and B , respectively. It is clear that for both cycles A and B , the entropy production $\Sigma(t)$ remains positive over time. Moreover, the entropy production in cycle A is smaller than that in cycle B over time. Physically, this indicates that the irreversibility of the total systems increases over time, where the decoherence effects of the reservoirs R_1 and R_2 are more pronounced in cycle B than in cycle A . This means the loss of information of QATM and the external systems is more remarkable in cycle B than in cycle A .

For the entropy production rate $\sigma(t)$, we observe a non-monotonic evolution over time for both cycles A and B . In addition, one can see that $\sigma(t)$ takes negative values during the evolution. Moreover, in cycle A , $\sigma(t)$ shows negative values more frequently and with greater amplitude than in cycle B . Physically speaking, negative values of the entropy production rate, i.e., $\sigma(t) < 0$ indicate the presence of non-Markovian dynamics during the evolution of the total system $M \otimes S$. Therefore, as previously mentioned, the fact that $\sigma(t)$ attains more negative values in cycle A suggests that the dynamics supports robust non-Markovianity in cycle A than in cycle B . Furthermore, increasing the coupling strength g between the QATM M and the external system S enhances the non-Markovian behavior, since larger g leads to more pronounced negative values of $\sigma(t)$ compared to smaller

g .

In the next section, we will examine the effect of the QATM cycle on the dynamics of the external system $S = S_1 \otimes S_2$. Indeed, we will identify the source of non-Markovianity and discuss the impact of these results on entanglement generation in the external system S .

IV. IMPACT OF MEMORY EFFECTS ON ENTANGLEMENT GENERATION IN QATM CYCLES FOR EXTERNAL SYSTEM QUBITS

As discussed before, the signature of non-Markovianity is observed through the oscillations in heat transfer, the temperature evolution of the QATM qubit, and the negative values of the entropy production rate. Hence, in this section, we will investigate the source of non-Markovianity and analyze the effect of QATM cycles A and B on entanglement generation and the role of coherence in the external system S .

A. Non-Markovianity and correlation exchanges between the QATM and the external system

In our paper [15], we showed that the QATM can induce a backflow of information (non-Markovianity) in the external system through the exchange of correlations between them. Similarly, the work introduced by Popovic

et al. [30] demonstrates that the non-Markovianity can emerge from the exchange of correlations between subsystems. In our scenario, we quantify non-Markovianity using the measure proposed by Breuer *et al.* [31], denoted by $\mathcal{N}_m(t)$. Indeed, it is based on the distinguishability between two quantum states, which are given in our case by $\hat{\rho}_m^\alpha(t)$ and $\hat{\rho}_m^\beta(t)$, for $m = \{M, S_1, S_2\}$. Mathematically, it is defined as:

$$\mathcal{N}_m(t) = \max_{\hat{\rho}_m^{\alpha\beta}(0)} \int_{\vartheta_m(t) > 0} dt \vartheta_m(t), \quad (22)$$

where $\hat{\rho}_m^{\alpha\beta}(0) = \hat{\rho}_m^\alpha(0) - \hat{\rho}_m^\beta(0)$, and $\vartheta_m(t) = \frac{d}{dt} \|\hat{\rho}_m^{\alpha\beta}(t)\|$ is the time derivative of the trace distance between $\hat{\rho}_m^\alpha(t)$ and $\hat{\rho}_m^\beta(t)$. However, we quantify the correlation between the QATM $M = M_1 \otimes M_2$ and the external system $S = S_1 \otimes S_2$ using quantum mutual information [32], namely $\mathcal{I}_{M \otimes S}(t)$, which is given as:

$$\mathcal{I}_{M \otimes S}(t) = S(\hat{\rho}_M(t)) + S(\hat{\rho}_S(t)) - S(\hat{\rho}(t)), \quad (23)$$

where $S(\hat{\rho}_m(t))$ is the von-Neumann entropy of the subsystem $m = \{M, S\}$. However, for the initial state of QATM M , we set $\hat{\rho}_M^\alpha(0) = \hat{\rho}_M^\beta(0) = \hat{\rho}_M(0)$, which is the same state used in Eq. (7). For the external system S , we take $\hat{\rho}_S^\alpha(0) = \hat{\rho}_S(0)$ and $\hat{\rho}_S^\beta(0) = \bar{\rho}_S(0)$, where $\hat{\rho}_S(0)$ is the same state used in Sec. III. The state $\bar{\rho}_S(0)$ is given as bellow:

$$\bar{\rho}_S(0) = \sum_{n_{S_1}, n_{S_2}=0}^1 \langle n_{S_1} n_{S_2} | \hat{\rho}_S(0) | n_{S_1} n_{S_2} \rangle | n_{S_1} n_{S_2} \rangle \langle n_{S_1} n_{S_2} |, \quad (24)$$

which represents the fully dephased (incoherent) state of the external system S in our computational basis.

In Fig. (5), we analyze the non-Markovianity measures $\mathcal{N}_M(t)$, $\mathcal{N}_{S_1}(t)$, and $\mathcal{N}_{S_2}(t)$ for the QATM M , external system qubit S_1 and S_2 , respectively. Moreover, we examine the mutual information $\mathcal{I}_{M \otimes S}(t)$ between M and S versus time and for various considerations of the strength g . For both cycles A and B , we observe that when the coupling g increases, the non-Markovianity also increases on the subsystems M , S_1 and S_2 . Furthermore, we observe that the quantum correlation increases when the coupling g takes large values. However, the non-Markovianity and correlation are higher in the case of cycle A than cycle B , which proves that negative entropy production rate values are a witness of non-Markovianity in our theoretical model. Also, the correlations in cycle A are dominant compared to cycle B , meaning that cycle A conserves the information of the subsystems more effectively than cycle B .

Hence, the memory effect in our theoretical model is due to the correlations exchanged between the QATM M and the external system S over time. Indeed, this correlation partially preserves the information between the subsystems over time. Effectively, one can conclude

that the QATM reacts as a quantum-structured non-Markovian reservoir with the reservoirs R_1 and R_2 . Physically speaking, this means that the QATM M acts as a filter of the decoherence effect of the reservoirs into the external system S .

B. Entanglement generation

The main subject of this work is to show the effect of the QATM by means of cycles A and B on the entanglement generation in the external system S over time. Indeed, to do this, we propose to quantify the amount of entanglement using the concurrence [33]. In fact, we aim to study the concurrence of the subsystems $S_1 \otimes S_2$, namely $\mathcal{C}_{S_1 \otimes S_2}(t)$. Moreover, for the sake of comparison, we also investigate the correlation between the external system qubits S_1 and S_2 using the mutual information, namely $\mathcal{I}_{S_1 \otimes S_2}(t)$. Indeed, they are expressed as [32]

$$\mathcal{C}_{S_1 \otimes S_2}(t) = \max[0, \sqrt{\lambda_1}(t) - \sum_{i=1}^4 \lambda_i(t)], \quad (25)$$

$$\mathcal{I}_{S_1 \otimes S_2}(t) = S(\hat{\rho}_{S_1}(t)) + S(\hat{\rho}_{S_2}(t)) - S(\hat{\rho}_S(t)), \quad (26)$$

where $\lambda_1(t) \geq \lambda_2(t) \geq \lambda_3(t) \geq \lambda_4(t)$ are eigenvalues of the spin-flipped density matrix $\hat{\rho}_S(t)(\sigma_{S_1}^y \otimes \sigma_{S_2}^y) \hat{\rho}_S^*(t)(\sigma_{S_1}^y \otimes \sigma_{S_2}^y)$. While, $S(\hat{\rho}_{S-i}(t))$ denotes the von-Neumann entropy of the qubit S_i for $i = \{1, 2\}$.

In Fig. (6), we analyze the entanglement and the correlations in the external system $S = S_1 \otimes S_2$ versus time. We set the coupling $g = 0.9$, and we show the behavior of $\mathcal{C}_{S_1 \otimes S_2}(t)$ and $\mathcal{I}_{S_1 \otimes S_2}(t)$ versus time and temperature $T_{M_2} \in [0.1T_{M_2}, T_{M_2}]$, to investigate the role of QATM M cycles on the entanglement and coherence generation in Figs. (6a) and (6b), respectively. We observe that if the temperature is below the white dashed line, which corresponds to $T_{M_1} < 0.5T_{M_2}$ in cycle A . Indeed, the concurrence increases as the temperature of qubit M_1 approaches $T_{M_1} = 0.1T_{M_2}$. If the temperature exceeds the white dashed line ($T_{M_1} \geq 0.5T_{M_2}$ for cycle B), the concurrence decreases and approaches zero compared to cycle A . In contrast, concerning the mutual information, we observe that there is a symmetric behavior with respect to the white dashed line, namely when $T_{M_1} = 0.5T_{M_2}$ that corresponds to the transition point between cycles A and B . Physically, this means that during the operation of cycle A of the QATM, the entanglement is generated, while the total correlation remains the same in both cycles A and B .

In Figs. (6c) and (6d), we show the impact of the coupling g on the dynamics of entanglement and correlation in the external system S , for cycles A and B , respectively. As we mentioned before, the total correlation in both cycles A and B is similar for all values of the coupling g . For the entanglement, we observe that in cycle A , entanglement is generated over time. While in cycle B , the concurrence has small values compared to cycle A .

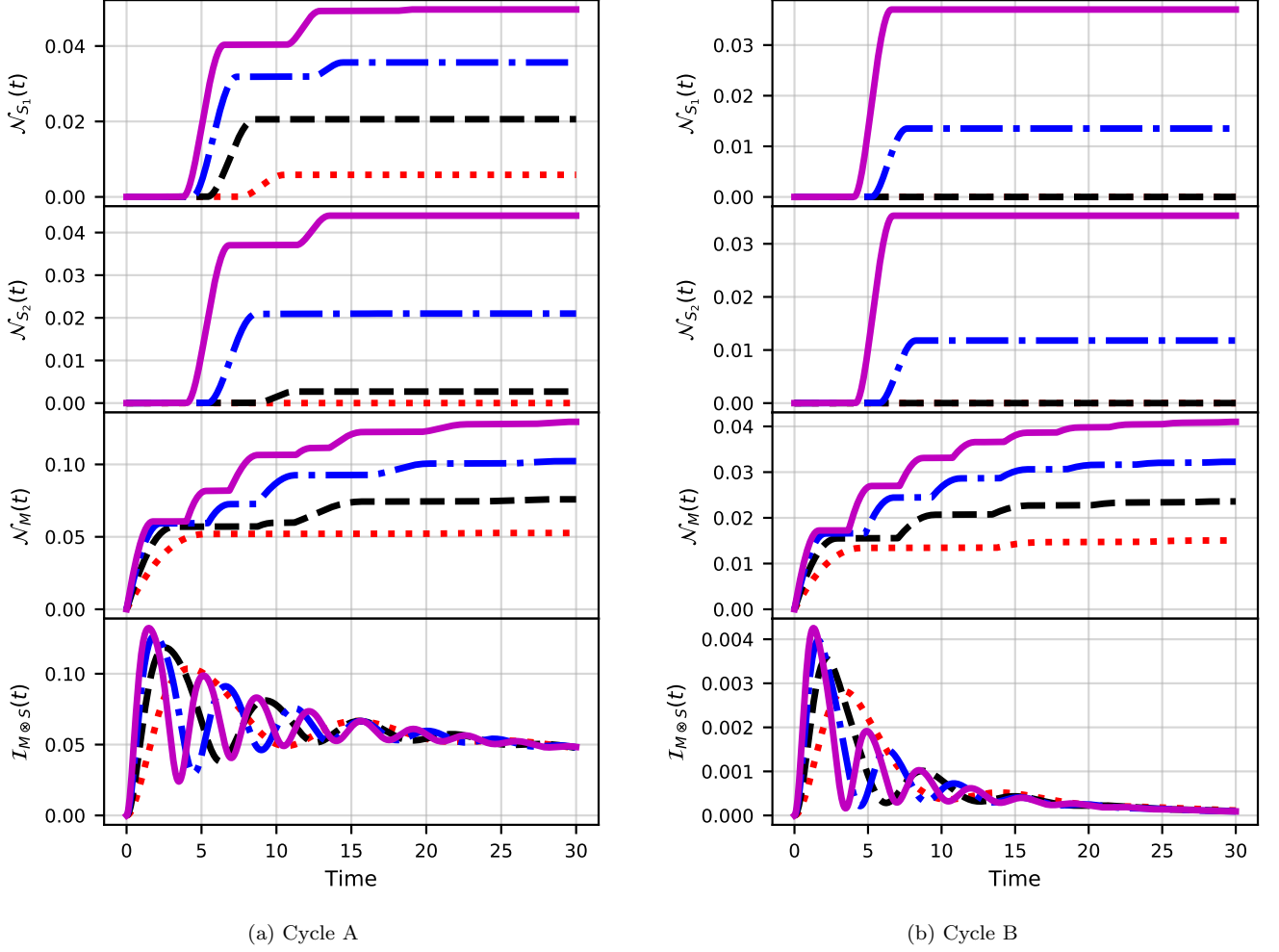


FIG. 5. Non-Markovianity measures and mutual information between the QATM and the external system. (a) Cycle A: robust non-Markovianity in all subsystems and stronger mutual information $I_{M \otimes S}(t)$ for large values of g is observed. (b) Cycle B: lower non-Markovianity and mutual information under the same coupling conditions. The coupling strength is varied in units of E_{M_2} as $g = 0.03, 0.05, 0.07$, and 0.09 for red, black, blue and magenta curves.

In addition, for any value of g , the concurrence behaviors are similar. But, they differ only in their monotonic evolution, since g is responsible for the non-Markovian dynamics in our theoretical model, as we showed in the previous parts.

C. Role of coherence correlation on entanglement generation

In this part, we show the role of coherence correlation, namely $\Delta C_S(t)$ and the local coherences of the external system qubit on the entanglement generation, for the two cycles A and B of the QATM. In fact, we investigate the relative entropy of coherence $C_{S_i}(t)$ for $i = \{1, 2\}$. Moreover, we examine the global relative entropy of coherence of $S = S_1 \otimes S_2$, namely $C_S(t)$. Indeed, they are defined as:

$$C_S(t) = S(\bar{\rho}_S(t)) - S(\hat{\rho}_S(t)), \quad (27)$$

$$C_{S_i}(t) = S(\bar{\rho}_{S_i}(t)) - S(\hat{\rho}_{S_i}(t)), \quad i = \{1, 2\}, \quad (28)$$

$$\Delta C_S(t) = C_S(t) - \sum_{i=1}^2 C_{S_i}(t), \quad (29)$$

where $S(\bar{\rho}_S(t))$ and $S(\bar{\rho}_{S_i}(t))$ are the von-Neumann entropies of the fully dephased states of the global system S and the local systems S_i for $i = \{1, 2\}$.

In Fig. (7), we analyze the role of coherence correlation $\Delta C_S(t)$ and local coherences $C_{S_i}(t)$ for $i = \{1, 2\}$ versus time. Indeed, these quantities for various considerations of the coupling between the QATM and the external system for cycles A and B are displayed in Figs. (7a) and (7b), respectively. Obviously, we observe that for both cycles A and B, the local coherences of the qubits S_1 and S_2 decrease non-monotonically. This means that

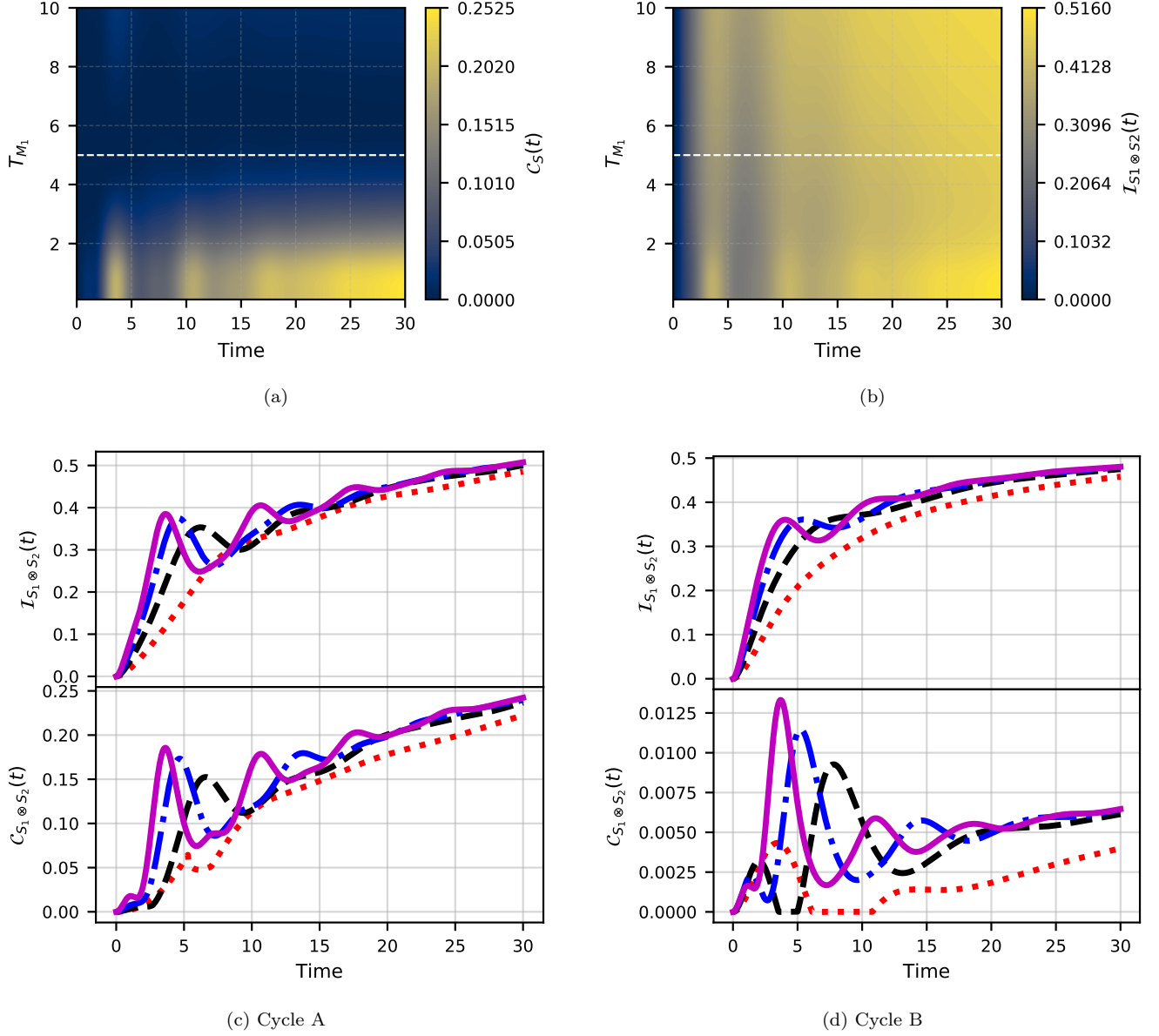


FIG. 6. Concurrence $C_{S_1 \otimes S_2}(t)$ and mutual information $I_{S_1 \otimes S_2}(t)$ between the external system qubits. (a,b) contour plots versus T_{M_1} and T_{M_2} , where the white dashed line separates cycles A and B. (c) Cycle A: noticeable entanglement amounts for different coupling values. (d) Cycle B: small entanglement amounts despite similar total correlations in (c). The coupling strength is varied in units of E_{M_2} as $g = 0.03, 0.05, 0.07$, and 0.09 for red, black, blue and magenta curves.

physically, there are memory effects during the coherence evolution. Moreover, the local coherence of the external subsystem in cycle B decays to zero more quickly than in cycle A, due to the higher presence of non-Markovianity in the case of cycle A.

Concerning the coherence correlation $\Delta C_S(t)$, we observe that it increases non-monotonically over time for both cycles, which means that the global coherence of the total external system S is larger than the local coherences of the external subsystems S_1 and S_2 , respectively, i.e., $C_S(t) > \sum_{i=1}^2 C_{S_i}(t)$. This is due to the exchange

of coherence correlation between the qubits S_1 and S_2 over time. Physically, there is a relationship between the total correlations quantified using mutual information $I_{S_1 \otimes S_2}(t)$, and the coherence correlation $\Delta C_S(t)$, which is given as below:

$$\Delta C_S(t) = I_{S_1 \otimes S_2}(t) - \bar{I}_{S_1 \otimes S_2}(t), \quad (30)$$

where $\bar{I}_{S_1 \otimes S_2}(t) = \sum_{i=1}^2 S(\bar{\rho}_{S_i}(t)) - S(\bar{\rho}_S(t))$ denotes the classical mutual information between the subsystems S_1 and S_2 , computed from the fully dephased states. These results show clearly the role of coherence corre-

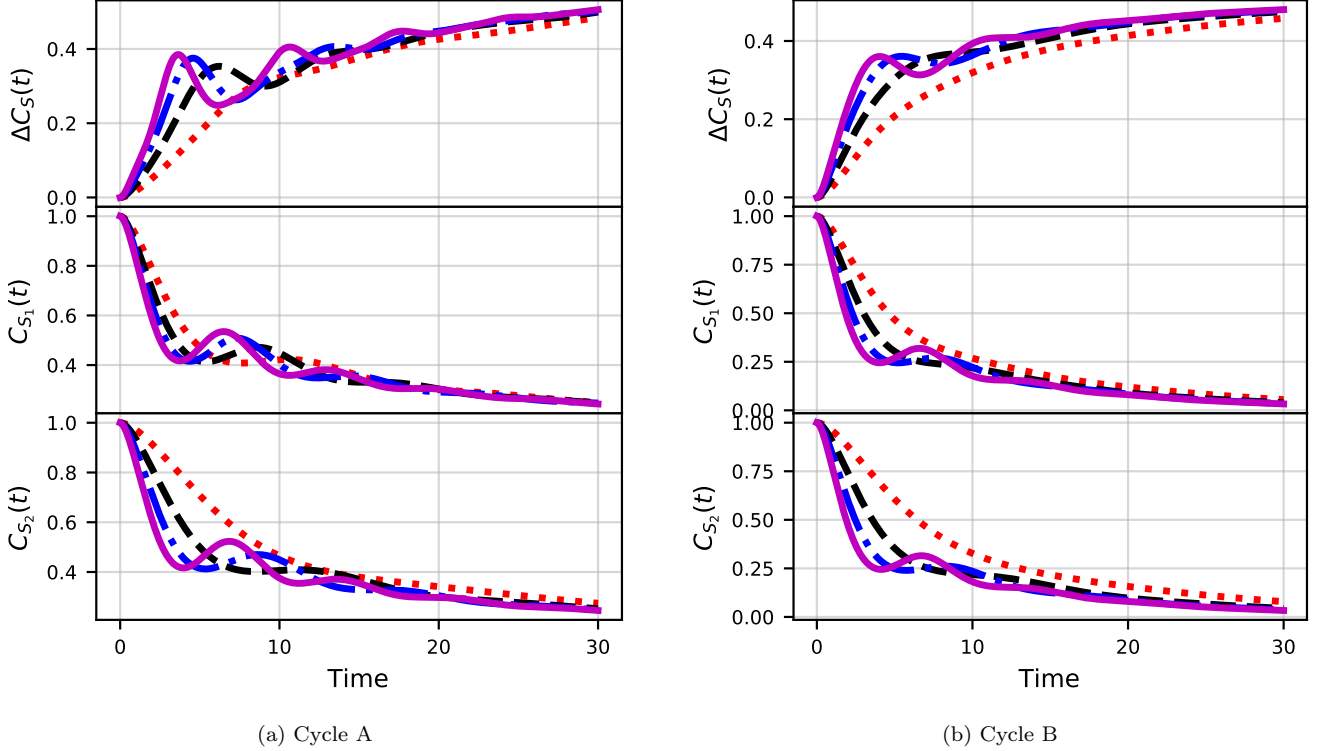


FIG. 7. Local coherences $C_{S_1}(t)$, $C_{S_2}(t)$ and coherence correlation $\Delta C_S(t)$ in the external system. (a) Cycle A: non-monotonic decay of local coherences with persistent and high coherence correlation. (b) Cycle B: faster decay of local coherences and lower coherence correlation, consistent with weaker non-Markovianity. The coupling strength is varied in units of E_{M_2} as $g = 0.03, 0.05, 0.07$, and 0.09 for red, black, blue and magenta curves.

lation in the creation of quantum correlations between S_1 and S_2 over time. Moreover, if the external systems S_1 and S_2 are incoherent, we obtain mathematically, $\mathcal{I}_{S_1 \otimes S_2}(t) = \bar{\mathcal{I}}_{S_1 \otimes S_2}(t)$, which means that the coherence correlation is vanished, namely $\Delta C_S(t) = 0$. Consequently, the concurrence is also vanished, which highlights the fact that entanglement is directly linked to coherence correlations. Hence, this confirms again our choice about the initial state of the external system qubits, which are initially prepared in superposition states.

V. DISCUSSION AND CONCLUSION

In this work, we explored, in a general context, the relationship between quantum thermodynamics theory in the framework of quantum thermal machines and quantum information theory by means of entanglement and non-Markovianity. We have studied the impact of the quantum autonomous thermal machine on entanglement generation, where we have considered the Hilbert space structure, temperatures, correlation exchange, memory effects, and correlation coherence as quantum resources. We show how the virtual temperature and energy spacing of the QATM and the external system

qubits are investigated to realize thermodynamical cycles A and B where we have demonstrated their effects on non-Markovianity and entanglement generation.

More precisely, we studied a quantum autonomous thermal machine composed of two qubits, namely M_1 and M_2 . Each qubit of the thermal machine is coupled in thermal equilibrium with its own bosonic Markovian reservoir, R_1 and R_2 , at different temperatures. However, an external system S which consists of two non-coupled qubits, S_1 and S_2 is also studied. Importantly, we investigated the Hilbert space structure and the notion of virtual temperature to realize a common coupling between QATM M and external system S . We provided the temperature and energy constraints necessary to realize thermodynamic cycles of QATM M . In fact, two cycles, A and B are represented, with the transition temperature between cycles is expressed in terms of the spacing energies E_{M_1} and E_{M_2} as $T_{M_1} = \frac{E_{M_2}}{E_{M_1}} T_{M_2}$. In this inspiration, we numerically demonstrated the robustness of our theoretical model by analyzing the QATM cycles based on heat exchange between QATM qubits M_1 , M_2 and external system qubits S_1 , S_2 . Furthermore, the impact of the temperatures T_{M_1} and T_{M_2} over time is also examined. We showed

that the transition from cycle A to B is characterized by the transition temperature $T_{M_1} = \frac{E_{M_2}}{E_{M_1}} T_{M_2}$. Then, we studied the second law of quantum thermodynamics using entropy production in our model. Hence, our results showed that the irreversibility in cycle A is smaller than that shown in cycle B , indicating that cycle A suppresses reservoir decoherence more efficiently.

Finally, we concluded that the entropy production rate can take negative values during evolution, which indicated the existence of memory effects. Hence, for more interpretations, we plotted the amount of non-Markovianity. Our results indicated that the non-Markovianity is more pronounced in cycle A than in cycle B , particularly in external qubits S_1 and S_2 . We concluded that this non-Markovianity resulted from the correlation exchange when QATM acts as a structured non-Markovian reservoir for S . However, we showed that the entanglement is generated in S only when QATM is operated in cycle A , due to lower irreversibility and higher non-Markovianity compared to cycle B . While the total correlation remained the same in both cycles, as it related to global properties of S . Indeed, these results demonstrated that cycle A controlled reservoir decoherence on S more effectively than cycle B . Hence, we concluded that correlation coherence is an essential resource for entanglement generation in S .

The results of our work are more general compared to those given in many references, particularly in Refs.[1, 7]. Indeed, in the literature, they investigated the steady-

state entanglement of QATM without external system or memory effects. Also, Aguilar *et al* [10] considered thermal machine entanglement in different environments, but they neglected the memory effects of the autonomous thermal machines. But, our model considered QATM in non-equilibrium and its effect on the external system with memory effects and Hilbert space structure to realize thermodynamical cycles, generalization based on our recent work [15] by exploring entanglement generation and quantum thermodynamic cycles beyond steady state. Finally, note that our theoretical model is suitable for superconducting qubit platforms, as parameters align with those used in existing experimental works.

ACKNOWLEDGMENTS

A. K acknowledges CNRST-Morocco support for this research within the Program " PhD-ASSociate Scholarship – PASS".

DECLARATION OF INTEREST

The authors declare that they have no conflict of interest.

DATA AVAILABILITY STATEMENT

No data statement is available.

-
- [1] N. M. Myers, O. Abah, and S. Deffner, "Quantum thermodynamic devices: From theoretical proposals to experimental reality," *AVS Quantum Sci.* **4**, 027101 (2022).
 - [2] R. Alicki and R. Kosloff, "Introduction to quantum thermodynamics: History and prospects," in *Thermodynamics in the Quantum Regime: Fundamental Aspects and New Directions*, edited by F. Binder, L. A. Correa, C. Gogolin, J. Anders, and G. Adesso (Springer, Cham, 2019), pp. 1–33.
 - [3] J. Millen and A. Xuereb, "Perspective on quantum thermodynamics," *New J. Phys.* **18**, 011002 (2016).
 - [4] S. Bhattacharjee and A. Dutta, "Quantum thermal machines and batteries," *Eur. Phys. J. B* **94**, 239 (2021).
 - [5] P. P. Hofer, J. A. B. Brask, M. Perarnau-Llobet, and N. Brunner, "Quantum thermal machine as a thermometer," *Phys. Rev. Lett.* **119**, 090603 (2017).
 - [6] R. S. Watson and K. Kheruntsyan, "Quantum many-body thermal machines enabled by atom-atom correlations," *SciPost Phys.* **18**, 190 (2025).
 - [7] S. Khandelwal, B. Annby-Andersson, G. F. Diotallevi, A. Wacker, and A. Tavakoli, "Maximal steady-state entanglement in autonomous quantum thermal machines," *npj Quantum Inf.* **11**, 28 (2025).
 - [8] J. B. Brask, G. Haack, N. Brunner, and M. Huber, "Autonomous quantum thermal machine for generating steady-state entanglement," *New J. Phys.* **17**, 113029 (2015).
 - [9] G. F. Diotallevi, B. Annby-Andersson, P. Samuelsson, A. Tavakoli, and P. Bakhshinezhad, "Steady-state entanglement production in a quantum thermal machine with continuous feedback control," *New J. Phys.* **26**, 053005 (2024).
 - [10] M. Aguilar, N. Freitas, and J. P. Paz, "Entanglement generation in quantum thermal machines," *Phys. Rev. A* **102**, 062422 (2020).
 - [11] R. Silva, G. Manzano, P. Skrzypczyk, and N. Brunner, "Performance of autonomous quantum thermal machines: Hilbert space dimension as a thermodynamical resource," *Phys. Rev. E* **94**, 032120 (2016).
 - [12] N. Linden, S. Popescu, and P. Skrzypczyk, "How small can thermal machines be? The smallest possible refrigerator," *Phys. Rev. Lett.* **105**, 130401 (2010).
 - [13] N. Brunner, N. Linden, S. Popescu, and P. Skrzypczyk, "Virtual qubits, virtual temperatures, and the foundations of thermodynamics," *Phys. Rev. E* **85**, 051117 (2012).
 - [14] A. Usui, W. Niedenzu, and M. Huber, "Simplifying the design of multilevel thermal machines using virtual qubits," *Phys. Rev. A* **104**, 042224 (2021).

- [15] A. Khoudiri, A. El Allati, Ö. E. Müstecaplıoğlu, and K. El Anouz, “Non-Markovianity and a generalized Landauer bound for a minimal quantum autonomous thermal machine with a work qubit,” *Phys. Rev. E* **111**, 044124 (2025).
- [16] A. E. Allahverdyan and T. M. Nieuwenhuizen, “Breakdown of the Landauer bound for information erasure in the quantum regime,” *Phys. Rev. E* **64**, 056117 (2001).
- [17] G. Gour, “Resources of the quantum world,” arXiv:2402.05474 [quant-ph] (2024).
- [18] E. Chitambar and G. Gour, “Quantum resource theories,” *Rev. Mod. Phys.* **91**, 025001 (2019). Y. Zhou, Q. Zhao, X. Yuan, and X. Ma, “Detecting multipartite entanglement structure with minimal resources,” *npj Quantum Inf.* **5**, 83 (2019).
- [19] J. Agustí, C. M. Schneider, K. G. Fedorov, S. Filipp, and P. Rabl, “Non-Markovian thermal reservoirs for autonomous entanglement distribution,” arXiv:2506.20742 [quant-ph] (2025).
- [20] G. Zambon and G. Adesso, “Quantum processes as thermodynamic resources: the role of non-Markovianity,” *Phys. Rev. Lett.* **134**, 200401 (2025).
- [21] M. H. Chakour, K. El Anouz, Y. Hassouni, and A. El Allati, “Improving different thermodynamic quantities in non-Markovian regime,” *Quantum Inf. Process.* **24**, 1 (2025).
- [22] H. Assil, A. El Allati, and G. L. Giorgi, “Entanglement estimation of Werner states with a quantum extreme learning machine,” *Phys. Rev. A* **111**, 022412 (2025).
- [23] M. T. Naseem and Ö. E. Müstecaplıoğlu, “Engineering entanglement between resonators by hot environment,” *Quantum Sci. Technol.* **7**, 045012 (2022).
- [24] G. De Chiara and M. Antezza, “Quantum machines powered by correlated baths,” *Phys. Rev. Res.* **2**, 033315 (2020).
- [25] P. Doyeux, B. Leggio, R. Messina, and M. Antezza, “Quantum thermal machine acting on a many-body quantum system: Role of correlations in thermodynamic tasks,” *Phys. Rev. E* **93**, 022134 (2016).
- [26] N. Brunner, M. Huber, N. Linden, S. Popescu, R. Silva, and P. Skrzypczyk, “Entanglement enhances cooling in microscopic quantum refrigerators,” *Phys. Rev. E* **89**, 032115 (2014).
- [27] M. S. Blok and G. T. Landi, “Quantum thermodynamics for quantum computing,” *Nat. Phys.* **21**, 187 (2025).
- [28] G. T. Landi and M. Paternostro, “Irreversible entropy production: From classical to quantum,” *Rev. Mod. Phys.* **93**, 035008 (2021).
- [29] S. Deffner and E. Lutz, “Nonequilibrium entropy production for open quantum systems,” *Phys. Rev. Lett.* **107**, 140404 (2011).
- [30] M. Popovic, B. Vacchini, and S. Campbell, “Entropy production and correlations in a controlled non-Markovian setting,” *Phys. Rev. A* **98**, 012130 (2018).
- [31] H. P. Breuer, E. M. Laine, and J. Piilo, “Measure for the degree of non-Markovian behavior of quantum processes in open systems,” *Phys. Rev. Lett.* **103**, 210401 (2009).
- [32] G. De Tomasi, S. Bera, J. H. Bardarson, and F. Pollmann, “Quantum mutual information as a probe for many-body localization,” *Phys. Rev. Lett.* **118**, 016804 (2017).
- [33] X. Meng, J. Gao, and S. Havlin, “Concurrence percolation in quantum networks,” *Phys. Rev. Lett.* **126**, 170501 (2021).
- [34] S. Chin, “Generalized coherence concurrence and path distinguishability,” *J. Phys. A: Math. Theor.* **50**, 475302 (2017).
- [35] D. Mondal, T. Pramanik, and A. K. Pati, “Nonlocal advantage of quantum coherence,” *Phys. Rev. A* **95**, 010301(R) (2017).
- [36] T. W. Crowther, H. B. Glick, K. R. Covey, C. Bettigole, D. S. Maynard, S. M. Thomas, *et al.*, “Correction: Corrigendum: Mapping tree density at a global scale,” *Nature* **532**, 268 (2016).
- [37] M. A. Aamir, P. Jamet Suria, J. A. Marín Guzmán, C. Castillo-Moreno, J. M. Epstein, N. Yunger Halpern, and S. Gasparinetti, “Thermally driven quantum refrigerator autonomously resets a superconducting qubit,” *Nat. Phys.* **21**, 318 (2025).
- [38] P. A. Erdman and F. Noé, “Identifying optimal cycles in quantum thermal machines with reinforcement-learning,” *npj Quantum Inf.* **8**, 1 (2022).
- [39] Y. Khelifi, A. El Allati, A. Salah, and Y. Hassouni, “Quantum heat engine based on spin isotropic Heisenberg models with Dzyaloshinskii–Moriya interaction,” *Int. J. Mod. Phys. B* **34**, 2050212 (2020).
- [40] A. El Allati, K. El Anouz, M. H. B. A. Chakour, and S. Al-Kuwari, “Non-Markovian effects on the performance of a quantum Otto refrigerator,” *Phys. Lett. A* **496**, 129316 (2024).
- [41] Y. Khelifi, S. Seddik, and A. El Allati, “Steady state entanglement behavior between two quantum refrigerators,” *Physica A* **596**, 127199 (2022).
- [42] M. H. B. Chakour, A. El Allati, and Y. Hassouni, “Entangled quantum refrigerator based on two anisotropic spin-1/2 Heisenberg XYZ chain with Dzyaloshinskii–Moriya interaction,” *Eur. Phys. J. D* **75**, 42 (2021).
- [43] B. M. H. Abdou Chakour, A. El Allati, and Y. Hassouni, “[Title not provided],” *Phys. Lett. A* **451**, 128410 (2022).
- [44] Y. Khelifi, A. El Allati, A. Salah, and Y. Hassouni, “Evaluating the performance of a refrigerator by an external system using entanglement,” *Eur. Phys. J. D* **75**, 195 (2021).